Contribution of Disulfide Bonds to Stability, Folding, and Amyloid Fibril Formation: The PI3-SH3 Domain Case

Ricardo Graña-Montes,[1,*] Natalia S. de Groot,[1,*] Virginia Castillo,[1] Javier Sancho,[2–4]
Adrian Velazquez-Campoy,[2–5] and Salvador Ventura[1]

Abstract

Aims: The failure of proteins to fold or to remain folded very often leads to their deposition into amyloid fibrils and is the origin of a variety of human diseases. Accordingly, mutations that destabilize the native conformation are associated with pathological phenotypes in several protein models. Protein backbone cyclization by disulfide bond crosslinking strongly reduces the entropy of the unfolded state and, usually, increases protein stability. The effect of protein cyclization on the thermodynamic and kinetics of folding has been extensively studied, but little is know on its effect on aggregation reactions. *Results:* The SRC homology 3 domain (SH3) of p85α subunit of bovine phosphatidyl-inositol-3'-kinase (PI3-SH3) domain is a small globular protein, whose folding and amyloid properties are well characterized. Here we describe the effect of polypeptide backbone cyclization on both processes. *Innovation:* We show that a cyclized PI3-SH3 variant is more stable, folds faster, aggregates slower, and forms conformationally and functionally different amyloid fibrils than the wild-type domain. *Conclusion:* Disulfide bridges may act as key molecular determinants of both productive protein folding and deleterious aggregation reactions. *Antioxid. Redox Signal.* 16, 1–15.

Introduction

PROTEIN MISFOLDING AND AGGREGATION is associated to an increasing number of human disorders, ranging from dementia to diabetes (13). The proteins involved in such pathologies are not related sequentially or structurally, but self-assemble into ordered amyloid fibrils sharing a common cross-β-sheet motif (23). This property is not an unusual feature exhibited by a reduced set of proteins, but is rather inherent to most, if not all, polypeptides (22, 28). Thus, in addition to the native fold, an alternative, stable, and ordered state is accessible to proteins. Both states compete in the cell, resulting in functional or toxic conformations depending on whether the native or the aggregated state is populated (30).

Because protein aggregation requires at least local backbone fluctuations and in many cases partial unfolding (12, 14), the deposition propensity of globular proteins appears to be linked to their thermodynamic and/or kinetic stability (10), in such a way that mutations or environmental conditions that destabilize the native structure or increase unfolding rates are

associated to pathological phenotypes in several protein models (6, 24). This could be one of the underlying reasons why proteins that function in harsh environments, such as the extracellular space, have evolved disulfide bonds (48). Natural disulfide bonds can stabilize proteins to a large extent and strongly reduce conformational fluctuations (1). In some cases, the stabilizing effect is so high that the protein readily unfolds when its disulfides are reduced (19). By crosslinking sequentially distant regions of the polypeptide chain, disulfide bonds are assumed to decrease the entropy of the unfolded ensemble, making it less favorable compared with the folded conformation. Thus, the maximum stabilization will be attained when the disulfide bond links the two termini of the molecule; natural proteins like cyclotides exploit this strategy to become exceptionally stable (9). Crosslinking the polypeptide chain affects not only the stability of the protein at equilibrium but also, in many cases, its mechanism and/or kinetics of folding (25, 49). In fact, engineering of new disulfide bonds and analysis of the corresponding changes in folding kinetics is a useful approach to

[1]Departament de Bioquímica i Biologia Molecular, Institut de Biotecnologia i de Biomedicina, Universitat Autònoma de Barcelona, Bellaterra (Barcelona), Spain.
[2]Departamento de Bioquímica y Biología Molecular, Universidad de Zaragoza, Zaragoza, Spain.
[3]Institute of Biocomputation and Physics of Complex Systems, Universidad de Zaragoza, Zaragoza, Spain.
[4]Unidad Asociada BIFI-IQFR, CSIC, Zaragoza, Spain.
[5]Fundación ARAID, Diputación General de Aragón, Zaragoza, Spain.
*These two authors contributed equally to this work.

Innovation

Cyclization significantly stabilizes SH3 domain of p85α subunit of bovine phosphatidyl-inositol-3′-kinase (PI3-SH3) and strongly accelerates its folding rate while having a minor effect on its unfolding rate, promoting the fast attainment of the folded state and a higher proportion of native molecules at equilibrium, contributing thus to decrease the population of aggregation-prone species. In addition, even when amyloidogenic intermediates are populated, cyclization slow downs PI3-SH3 self-assembly and renders the fibrils less cytotoxic. Thus, disulfide bonds likely reduce the chances of pathogenic protein aggregation, especially in the extracellular space, where polypeptides are not subjected to the surveillance of molecular chaperones. Prevention of protein aggregation is an important selective pressure acting on the evolution of protein sequences (11); the protective effect of disulfide bonds against toxic protein deposition in the oxidative extracellular background might explain why the sequences of secreted SH3 domains can support a higher intrinsic aggregation load than those of their less stable intracellular counterparts. Importantly, during the revision of this work, a study by Mossuto *et al.* showed that reduction of disulfides in human lysozyme increases the toxicity of the resulting fibrils and, more generally, that disulfide-containing proteins in the human proteome display a high aggregation propensity (36). Overall, it appears that the impact that covalent polypeptide crosslinking exerts in the complex processes of protein folding and aggregation might be more relevant from the physiological point of view than previously thought. In this sense, the design of new disulfide bonds might be an effective strategy to reduce the aggregation of target proteins of biotechnological interest.

study the proximity of specific protein regions in the transition state ensemble (27).

SRC homology 3 domain (SH3) domains are good model systems for folding and aggregation analysis due to their monomeric state, their small size, and the absence of cofactors and, usually, disulfide bonds. The SH3 domain of p85α subunit of bovine phosphatidyl-inositol-3′-kinase (PI3-SH3) consists of 83 residues that fold into five β-strands and two short helix-like turns. The five β-strands are arranged in two β-sheets that are orthogonal to each other forming a β-sandwich (33) (Fig. 1). PI3-SH3 appears to fold/unfold following a canonical two state mechanism (49), although recent studies suggest the existence of a transient intermediate after the rate-limiting step of folding (47). PI3-SH3 constitutes one of the best-characterized globular proteins able to form ordered amyloid fibrils starting from an acid-unfolded state (28, 46). Therefore, this domain provides a framework to study the effect of backbone cyclization on protein stability, folding, and aggregation.

Here, we investigate the properties of a PI3-SH3 mutational variant in which the N- and C- termini have been crosslinked by a designed disulfide bond. Overall, the data collected here indicate that, by altering polypeptide chain connectivity, disulfide bridges have a high impact in protein folding as well as in amyloid formation and suggest that they may play a major role in minimizing misfolding and aggregation phenomena.

Results

Crosslinking the N and C termini in the PI3-SH3 domain

We used FoldX (42) to design a PI3-SH3 domain with the N and C terminal ends linked by a disulfide bridge. We searched for two residues close enough in the native structure to permit the formation of the desired covalent interaction after their mutation to Cys. The best positions were Ala3 and Ile82, due to their proximity (distance between the β-carbons = 4.2 Å), face-to-face orientation, and proper dihedral angles. Therefore, we cloned, produced, and purified an SH3-PI3 mutant with both residues replaced by Cys (PI3-SH3-SS). The absence of detectable alkylation by vinylpyridine confirmed the formation of the designed disulfide bond. The introduced covalent linkage closes off a loop of 78 residues (Fig. 1).

Conformational analysis of PI3-SH3 domains under native conditions

The wild-type domain (PI3-SH3-WT) and PI3-SH3-SS exhibit analogous far-UV circular dichroism (CD) spectra under native conditions (pH 7.0 and 298 K) with a characteristic minimum at 222 nm (46) (Fig. 2A). However, the PI3-SH3-WT maximum at 235 nm is absent in PI3-SH3-SS. The far-UV CD spectrum of PI3-SH3-SS under reducing conditions does not change significantly, suggesting that the change in the spectrum is associated to the sequential changes and not to disulfide bond promoted strain. Accordingly, Cys residues are known to contribute negatively to the CD signal of peptides in this region of the spectrum (32). We will refer to PI3-SH3-SS in its reduced form as PI3-SH3-(SH)$_2$.

PI3-SH3 contains a single Trp in position 55 and 4 Tyr residues at positions 6, 8, 12, and 59. We excited the different proteins at 268 nm and recorded their intrinsic fluorescence emission spectra under native and reducing conditions. No significant differences were detected between domains (Fig. 2B). The structural features of the PI3-SH3-WT and PI3-SH3-SS were also evaluated by NMR spectroscopy. The one-dimensional NMR (^{1}H-NMR) spectrum of both proteins at pH 7.0 and 298 K display a wide signal dispersion of resonances at both low (amide and aromatic region) and high (methyl region) fields, with good peak sharpness, characteristic of folded molecules (Fig. 3). The two spectra are almost identical, which together with the CD and fluorescence data indicate that the introduced mutations do no affect significantly the PI3-SH3-fold.

Thermal unfolding of PI3-SH3 domains

The thermal stability of PI3-SH3 domains at pH 7.0 was analyzed by intrinsic fluorescence, CD, differential scanning calorimetry (DSC), and ^{1}H-NMR (Fig. 4).

The transition curves from heat-induced fluorescence emission changes in PI3-SH3 domains are shown in Figure 4A. The thermal denaturation curves followed by far-UV CD at 235 nm are show in Figure 4B. In both cases a single cooperative transition was observed and the data could be fitted accurately to a two-state temperature-induced unfolding
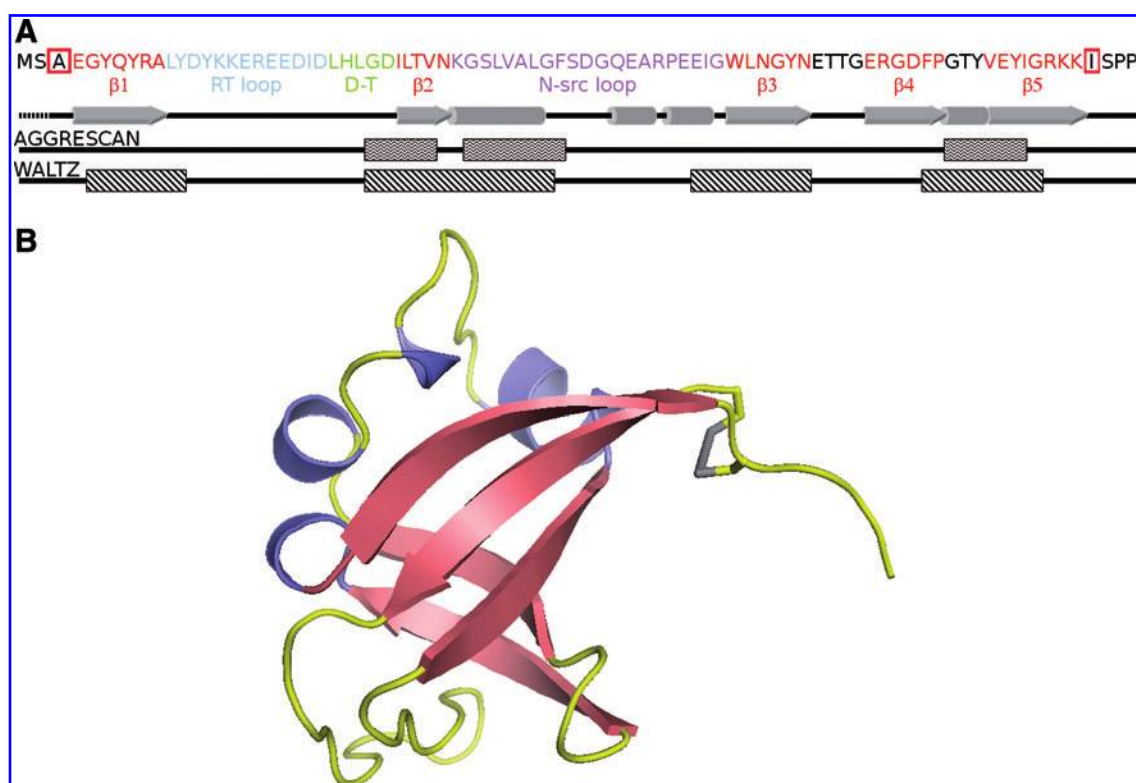
FIG. 1. **SH3 domain of p85α subunit of bovine phosphatidyl-inositol-3′-kinase (PI3-SH3)-WT. (A)** Sequence, SH3-fold characteristic structural features are depicted with different colors; the positions mutated by Cys are shown within *red squares*. The diagram below represents the distribution of secondary structure elements along the sequence. Aggregation-prone regions of PI3-SH3-WT predicted with AGGRESCAN and WALTZ are shown as wavy and diagonal lines, respectively. **(B)** Structural model of PI3-SH3-SS (1PHT.pdb), sulfur atoms forming the disulfide bond of the mutated PI3-SH3 domain are colored in gray. The model was generated using PyMol. (To see this illustration in color the reader is referred to the web version of this article at www.liebertonline.com/ars.)

model ($R > 0.99$). DSC scans of PI3-SH3 exhibited a single cooperative transition corresponding to a two-state unfolding process without a significant population of intermediate partially unfolded states, according to the ratio between the van't Hoff and calorimetric enthalpies (Fig. 4C). As shown in Table 1, the transition temperatures of unfolding obtained by the three independent methods are very similar, coinciding to indicate that PI3-SH3-SS is considerably more stable toward thermal denaturation than the wild-type and reduced forms. PI3-SH3-$(SH)_2$ is somewhat more stable than the wild-type domain.

The temperature-induced unfolding of PI3-SH3-WT and PI3-SH3-SS was also analyzed by monitoring the changes in their ^{1}H-NMR spectra (Fig. 3). PI3-SH3-WT displays native signal dispersion and peak sharpness until 318 K; above this temperature the intensity of the signals steadily decays until at 338 K the spectrum collapses and the resonances at low fields are hardly detectable, indicating the absence of a preferential folded conformation. In the case of PI3-SH3-SS, the spectra remain essentially unchanged until 328 K and even at 338 K the spectrum presents good signal dispersion, although with decreased peak intensity. Both proteins appear to be completely unfolded at 358 K (data not shown). The area of the NMR signals in the aliphatic region was plotted against temperature and the resultant curves were adjusted to a two-state model (Fig. 4D). The derived melting temperatures

confirm the stabilization of the PI3-SH3-SS domain against thermal unfolding (Table 1).

Equilibrium denaturation of PI3-SH3 domains

The urea denaturation at equilibrium of the different PI3-SH3 domains was analyzed at pH 7.0 and 298 K. Protein unfolding was monitored by following the changes in intrinsic fluorescence at increasing urea concentrations. All three domains display a single detectable transition indicating the cooperativity of the unfolding process (Fig. 5A). The main thermodynamic parameters of the unfolding reaction were calculated from the equilibrium curves assuming a two-state model ($R > 0.99$ in both cases) (Table 2). The stability of PI3-SH3-WT is 4.4 kcal/mol with a [urea]$_{50\%}$ of 3.8 M. In agreement with the thermal denaturation data, PI3-SH3-$(SH)_2$ is slightly more stable. Both domains display similar m-values. The value of [urea]$_{50\%}$ for PI3-SH3-SS is $\sim 7.5\,M$; this value is so high that a final baseline for the fully unfolded state cannot be accurately measured and the m-value could not be determined. Therefore, we used guanidine hydrochloride (Gdn·HCl) for equilibrium denaturation of PI3-SH3-SS and compared it with that of the two other domains using the same denaturant (Fig. 5B). As detailed in Table 2, crosslinking stabilizes PI3-SH3-SS by ~ 3.5 kcal/mol relative to PI3-SH3-WT and shifts [Gdn·HCl]$_{50\%}$ from 1.7 to
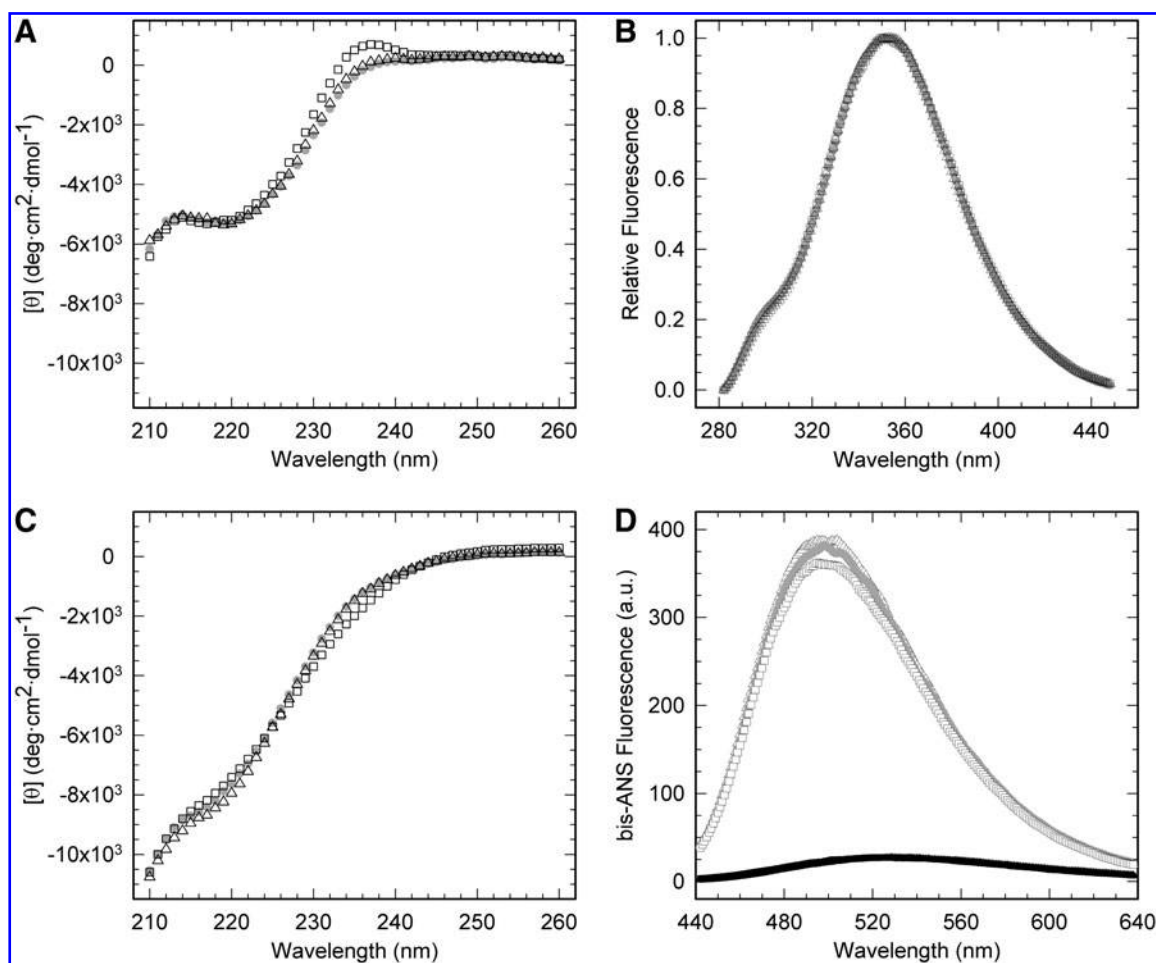
FIG. 2. Conformational analysis of PI3-SH3 domains. (A) Far-UV circular dichroism (CD) spectra at pH 7. **(B)** Intrinsic fluorescence emission spectra upon excitation at 268 nm at pH 7. **(C)** Far-UV CD spectra at pH 2. **(D)** 4,4′-dianilino-1,1′-binaphthyl-5,5′-disulfonic acid (bis-ANS) binding at pH 2. PI3-SH3-WT (*squares*), PI3-SH3-SS (*solid gray circles*), and PI3-SH3-$(SH)_2$ (*triangles*). In **(D)** bis-ANS binding to SH3 domains under native conditions is indicated with *solid black symbols*.

2.9 *M*. Overall, thermal and chemical denaturation data co-incide to indicate that the introduced 3–82 disulfide bond is strongly stabilizing both relative to the wild-type and the dithiol forms and therefore that the mutations are sterically acceptable.

Folding and unfolding kinetics of PI3-SH3 domains

The kinetics of folding and unfolding of the different PI3-SH3 domains were determined by stopped-flow at neutral pH and 298 K under a wide range of denaturant conditions. In all cases, the folding and unfolding traces by fluorescence fit well into single exponentials, indicating the lack of detectable intermediates according with a two-state model. The chevron plots for the different domains appear to be linear in the complete range of urea concentrations studied (Fig. 6). The rate constants for folding (k_f) and unfolding (k_u) and their dependence on the denaturant concentration (m_f and m_u) are shown in Table 3. The kinetic data agree with the equilibrium stabilities. Interestingly, PI3-SH3-SS folds over 35 times faster than PI3-SH3-WT (Fig. 6). This high acceleration of the folding reaction can be univocally attributed to the presence of the covalent bond, since PI3-SH3-$(SH)_2$ exhibits a k_f close to that of

the wild-type domain. In contrast, cyclization has only a minor effect on the unfolding rate. The calculated Φ_{F-U} value of 0.85 for the disulfide crosslink suggested that the N and C termini might be ordered in the transition state for folding. We analyzed the folding and unfolding kinetics of Y8A and V74A mutants in the N- and C-terminal β-strands to probe the degree of association between PI3-SH3-WT ends in the transition state (Fig. 6B). The side-chains of Tyr8 and Val47 face each other in the native structure. The two mutations are highly destabilizing (Table 3), indicating that these residues play an important role in maintaining the native conformation. However, the Φ_{F-U} values of 0.16 and 0.20 calculated for Y8A and V74A, respectively, indicate that, in the wild-type domain, the terminal β-strands 1 and 5 are not part of the folding nucleus.

Reductive unfolding and oxidative folding

In the presence of 1 m*M* dithiothreitol (DTT), the disulfide bond in native PI3-SH3-SS is completely reduced in less than 1 min, indicating that it is highly exposed to solvent (Supplementary Fig. S1A; Supplementary Data are available online at www.liebertonline.com/ars). *In vitro*, the oxidative folding reaction of PI3-SH3-$(SH)_2$ from denatured state is very inefficient,
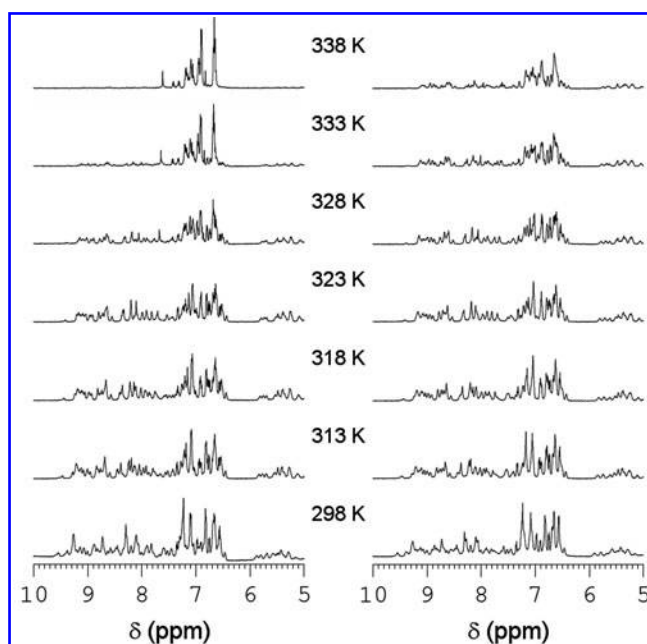
FIG. 3. ¹H-NMR spectra of PI3-SH3-WT (left) and PI3-SH3-SS (right) at the indicated temperatures.

taking more than 120 min even in the presence of an oxidizing agent such as 1 mM GSSG (Supplementary Fig. S1B). As shown above, the conformational folding of PI3-SH3-(SH)$_2$ occurs in seconds, indicating that the formation of the disulfide bond is the rate-limiting step of the oxidative folding reaction. This suggests that, in the reduced state, the free cysteine residues possess high degree of flexibility, which renders more difficult their oxidation to form the intramolecular disulfide bond.

Conformational analysis of PI3-SH3 domains at low pH

PI3-SH3-WT readily forms amyloid-like fibrils *in vitro* when incubated under acidic conditions. At pH 2.0 the CD spectra of all three domains display transitions to more un-folded conformations (Fig. 2C). These transitions do not re-flect global unfolding, as when adding a strong chemical denaturant, but rather partial unfolding, since it is known that at pH 2.0 PI3-SH3-WT forms the so-called A-state, a confor-mation that is more compact that the denatured state but less than the native one (28, 46). The A-state contains little sec-ondary structure and exposes hydrophobic surfaces to sol-vent; a property that can be monitored using 4,4'-dianilino-1,1'-binaphthyl-5,5'-disulfonic acid (bis-ANS). The A-state, from which amyloid assembly starts, seems to be accessible to the three domains, since in all cases we could detect a sig-nificant increase in the fluorescence emission of bis-ANS and a blue shift of its λ_{max} in the presence of the proteins at low pH (Fig. 2D). The native domains had a negligible effect on the spectral properties of the dye.
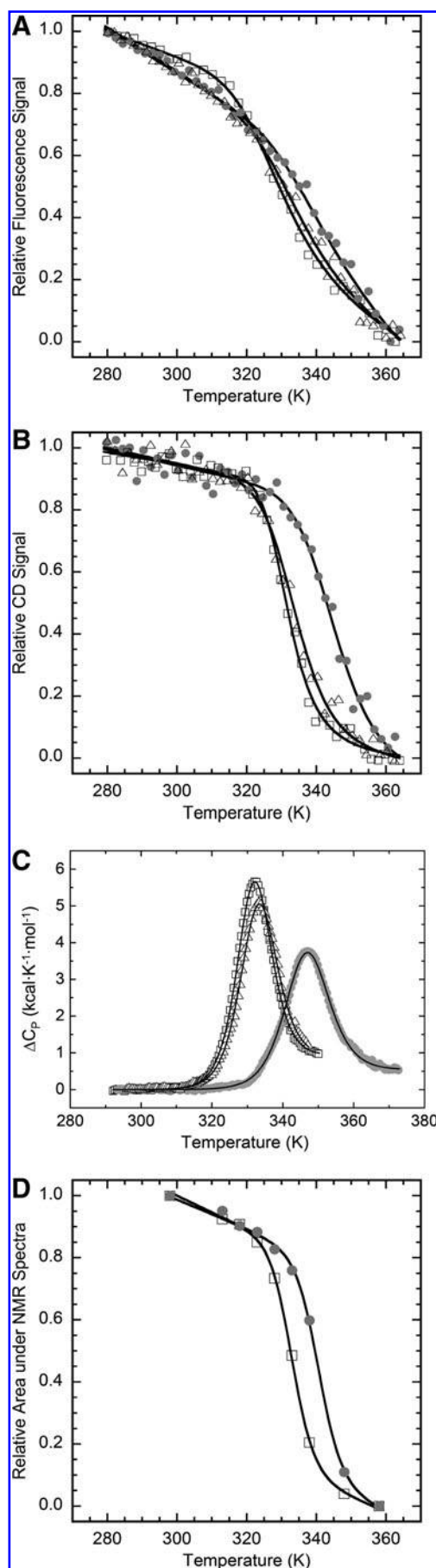
FIG. 4. Thermal unfolding followed by (A) intrinsic fluorescence, (B) far-UV CD, (C) differential scanning cal-orimetry, and (D) ¹H-NMR of PI3-SH3-WT (*squares*), PI3-SH3-SS (*solid gray circles*), and PI3-SH3-(SH)$_2$ (*triangles*). Nonlinear fit curves are represented by continuous lines.

TABLE 1. THERMAL DENATURATION THERMODYNAMIC PARAMETERS

	ΔH (T_m) $(kcal/mol)^a$	ΔC_p $(kcal/K \cdot mol)^a$	T_m $(K)^a$	T_m $(K)^b$	T_m $(K)^c$	T_m $(K)^d$
PI3-SH3-WT	67 ± 3	0.9 ± 0.2	331.2 ± 0.5	331.1 ± 0.3	331.9 ± 0.1	332.2 ± 0.2
PI3-SH3-SS	57 ± 3	0.5 ± 0.2	346.0 ± 0.5	345.2 ± 2.1	345.1 ± 0.2	342.1 ± 0.6
PI3-SH3-(SH)$_2$	63 ± 3	0.9 ± 0.2	332.4 ± 0.5	334.9 ± 0.4	333.9 ± 0.1	—

[a]DSC.
[b]Intrinsic fluorescence.
[c]CD.
[d]1H-NMR.
ΔC_p, heat capacity change of unfolding; CD, circular dichroism; DSC, differential scanning calorimetry; PI3-SH3, SH3 domain of p85α subunit of bovine phosphatidyl-inositol-3′-kinase.

Sequential aggregation propensity of PI3-SH3 domains

We used AGGRESCAN (18) and WALTZ (35) algorithms to estimate the effect of mutations on the intrinsic aggregation propensity of PI3-SH3. AGGRESCAN predicts three identical aggregation-prone regions for the wild-type and mutant proteins, comprising residues G27-V32, G35-F42, and G71-I77

FIG. 5. Equilibrium unfolding in the presence of (A) urea and (B) guanidine hydrochloride (Gdn·HCl) of PI3-SH3-WT (*squares*), PI3-SH3-SS (*circles*), and PI3-SH3-(SH)$_2$ (*triangles*).

(Fig. 1A). The first and last regions correspond with the second and last β-strands and the second region to the α-helix at the N-src loop. This algorithm calculates aggregation propensities of -19.9 and -20.7 for PI3-SH3-WT and PI3-SH3-(SH)$_2$, respectively. WALTZ identifies four identical amyloid-prone regions in both domains (Fig. 1A), comprising residues G5-Y12 in β-strand 1, G27-G41 in the RT-loop, E52-N60 in the N-src loop, and β-strand 3 and F69-G78 in the last β-strand. Overall, the introduced mutations are not expected to promote by themselves large changes in the aggregation propensity of the domain.

Amyloid fibril formation by PI3-SH3 domains

We analyzed the kinetics of PI3-SH3 domains amyloid fibril formation at acidic pH by monitoring the changes over time in the fluorescence of the amyloid staining dye Th-T (Fig. 7). In all cases we obtained characteristic polymerization sigmoidal curves, reflecting a nucleation-polymerization process that can be analyzed as an autocatalytic reaction (40). In agreement with the theoretical predictions, PI3-SH3-WT and PI3-SH3-(SH)$_2$ aggregation curves overlap exhibiting similar nucleation (7.10×10^3 s^{-1} and 6.29×10^3 s^{-1}, respectively) and elongation rates (1.76×10^{-3} M^{-1} s^{-1} and 1.02×10^{-3} M^{-1} s^{-1}, respectively). In contrast, the aggregation reaction of PI3-SH3-SS is significantly slower, with a 7-fold slower nucleation rate (1.01×10^3 M^{-1} s^{-1}) and 4-fold slower elongation rate (4.09×10^{-4} M^{-1} s^{-1}) than the wild-type protein.

Analysis of the different aggregation reactions by transmission electron microscopy (TEM) (Fig. 8) shows that the formation of protofibrilar aggregates in PI3-SH3-SS samples is
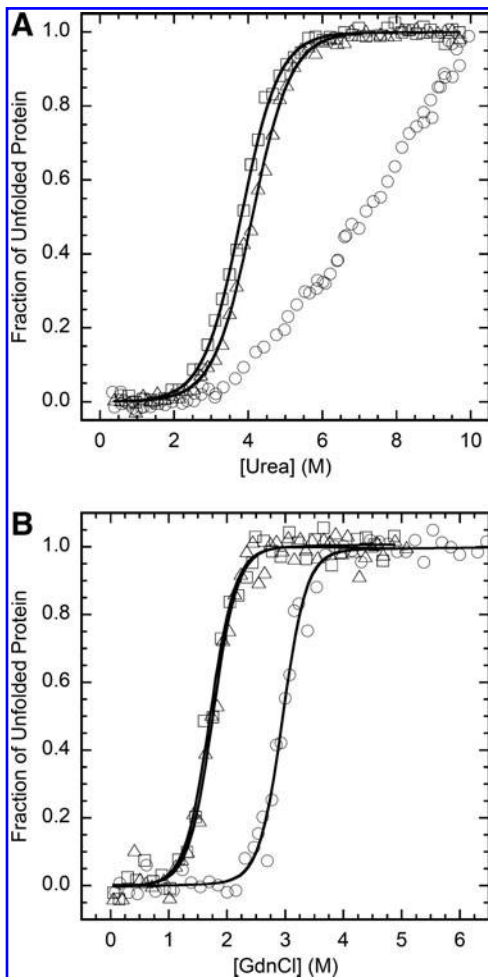
TABLE 2. THERMODYNAMIC PROPERTIES OF EQUILIBRIUM UNFOLDING OF PI3-SH3 DOMAINS

Domain/denaturant	$[]_{50\%}$ (M)	ΔG_{U-F} (kcal/mol)	m (kcal/molM)	$\Delta\Delta G_{U-F}$
PI3-SH3-WT/Urea	3.8	4.43 ± 0.22	1.16 ± 0.05	—
PI3-SH3-(SH)$_2$/Urea	4.1	4.67 ± 0.20	1.14 ± 0.05	0.24
PI3-SH3-SS/Urea	~ 7.5	—	—	—
PI3-SH3-WT/GdmCl	1.7	4.76 ± 0.81	2.74 ± 0.42	—
PI3-SH3-(SH)$_2$/GdmCl	1.8	4.92 ± 0.71	2.80 ± 0.36	0.16
PI3-SH3-SS/GdmCl	2.9	8.34 ± 1.13	2.81 ± 0.37	3.58

ΔG_{U-F} (free energy of unfolding) and $\Delta\Delta G_{U-F}$ (the difference in ΔG_{U-F} between the particular mutant protein and WT) were calculated from the equilibrium parameters as described in the Materials and Methods section.
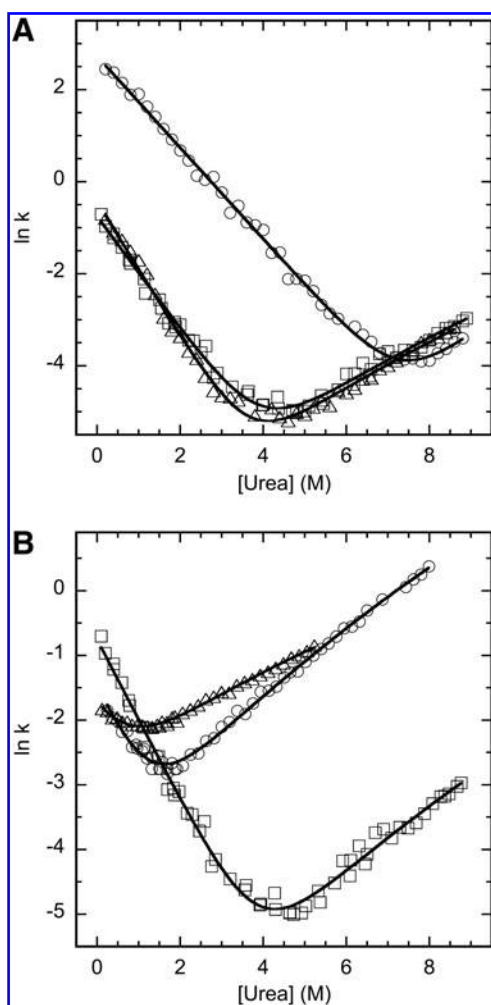
FIG. 6. Folding and unfolding kinetics. (A) Dependence of the folding and unfolding rate constants (k) on urea concentration of PI3-SH3-WT (*squares*), PI3-SH3-SS (*circles*), and PI3-SH3-(SH)$_2$ (*triangles*). **(B)** Dependence of the folding and unfolding rate constants (k) on urea concentration of PI3-SH3-WT (*squares*), Y8A (*triangles*), and V74A (*circles*) mutants.

delayed relative to that in PI3-SH3-WT and PI3-SH3-(SH)$_2$ solutions. After 42 h incubation, the three domains form typical amyloid fibrils (Fig. 8). However, differences in the morphology of the fibrils were observed. PI3-SH3-WT and

PI3-SH3-(SH)$_2$ fibrils were long and eventually tended to twist around each other, whereas PI3-SH3-SS formed shorter, discrete, and straight structures (Fig. 8). No evident depolymerization or shift in morphology could be observed when mature PI3-SH3-SS fibrils were incubated for 5 h under reducing conditions (data not shown).

Conformational and toxicity properties of PI3-SH3 amyloid fibrils

The conformational stability of the fibrils formed by the different domains after 42 h was assessed by equilibrium chemical denaturation with Gdn·HCl at pH 2.0 and 298 K following the changes in Th-T fluorescence (Fig. 9A) and light scattering (Fig. 9B). The fibrils seem to denature in a cooperative manner. The [Gdn·HCl]$_{50\%}$ calculated by measuring Th-T fluorescence were 3.2, 2.4, and 2.2 for PI3-SH3-SS, PI3-SH3-(SH)$_2$, and PI3-SH3-WT fibrils, respectively. Light scattering measurements rendered [Gdn·HCl]$_{50\%}$ values of 3.9, 3.1, and 2.9 for PI3-SH3-SS, PI3-SH3-(SH)$_2$, and PI3-SH3-WT fibrils, respectively. Therefore, the fibrils of PI3-SH3-SS appear to be more stable than those of the wild-type and reduced forms. In all cases, the stability calculated from Th-T measurements is lower than that obtained from light scattering. The difference in the two transition midpoints suggests the presence of intermediate states in which the ordered β-sheet is disrupted, in such a way that it does not longer bind Th-T, but still remains in an aggregated state, contributing thus to the light scattering signal. The population of these species can be approximated from the normalized denaturation data and fitted to a Gaussian distribution (Fig. 9C). The intermediate species distributions suggest that the β-sheet structure in the wild-type fibrils is less stable than in the fibrils of the disulfide crosslinked domain. To further explore whether the observed differences in fibrils morphology and stability are related to differences in the interactions supporting their architecture, we analyzed the conformational properties of PI3-SH3 mature fibrils by attenuated total reflectance–Fourier transformed infrared spectroscopy (ATR-FTIR) and bis-ANS binding and limited proteolysis. The ATR-FTIR spectra of all three fibrils in the amide I region is dominated by a main band at 1615–1640 cm^{-1} corresponding to β-sheet conformations (Fig. 9D–F). The secondary structure composition of PI3-SH3-WT (Fig. 9D) and PI3-SH3-(SH)$_2$ (Fig. 9E) fibrils are almost identical and differ from that of PI3-SH3-SS fibrils (Fig. 9F). The proportion of amyloid-like intermolecular β-sheet secondary structure is higher in the fibrils formed by PI3-SH3-SS (72%) than in those

TABLE 3. FOLDING KINETIC PARAMETERS FOR PI3-SH3 DOMAINS

Domain	$k_f^{0.5M}$ (s^{-1})	k_u^{8M} (s^{-1})	m_f (kcal/molM)	m_u (kcal/molM)	$-RT_{mF-U}$ (kcal/molM)	ΔG_{U-F} (kcal/mol)	$\Delta\Delta G_{U-F}$
PI3-SH3-WT	0.256 ± 0.013	0.0825 ± 0.0102	1.28 ± 0.03	0.51 ± 0.02	1.07 ± 0.03	4.39	—
PI3-SH3-(SH)$_2$	0.311 ± 0.019	0.0794 ± 0.0099	1.37 ± 0.03	0.58 ± 0.02	1.15 ± 0.03	4.62	0.23
PI3-SH3-SS	9.312 ± 0.389	0.0472 ± 0.0356	1.03 ± 0.03	0.75 ± 0.10	1.05 ± 0.07	8.04	3.65
Y8A	0.135 ± 0.005	0.8537 ± 0.0286	1.35 ± 0.11	0.45 ± 0.08	1.07 ± 0.10	0.09	-4.30
V74A	0.128 ± 0.007	1.4331 ± 0.0596	1.44 ± 0.08	0.67 ± 0.08	1.25 ± 0.08	1.52	-2.87

Kinetics of folding and unfolding were followed by changes in intrinsic fluorescence on a stopped flow instrument at 298 K; k_f is reported in 0.5 M urea and k_u is in 8 M urea to avoid extrapolation; m_f and m_u are the dependences of the folding and the unfolding rates, respectively, on urea. ΔG_{U-F} (free energy of unfolding) and $\Delta\Delta G_{U-F}$ (the difference in ΔG_{U-F} between the particular mutant protein and WT) were calculated from the kinetic parameters as described in the Materials and Methods section.
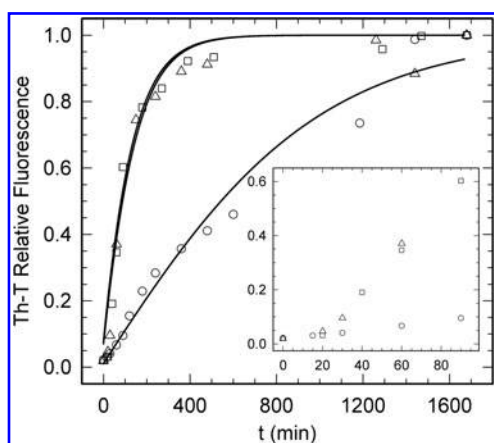
FIG. 7. **Aggregation kinetics under acidic conditions of PI3-SH3-WT (*squares*), PI3-SH3-SS (*circles*), and PI3-SH3-(SH)₂ (*triangles*).** The *inset* corresponding to the first 100 min shows the aggregation lag phase for the three domains.

the fibrils formed by PI3-SH3-SS (Fig. 9G). Accordingly, we observed that, in our conditions, the PI3-SH3-SS fibrils were totally resistant to pepsin digestion, whereas the wild-type fibrils were susceptible to proteolysis (Fig. 9H).

The toxicity of amyloid fibrils is related to their conformational properties. It has been shown for different and unrelated proteins that the binding to ANS-like dyes correlates with the toxicity of amyloid species, suggesting that the exposure of hydrophobic regions is a critical characteristic of these pathogenic assemblies (5). Although the aggregation of PI3-SH3 is not associated to any known disease, its amyloid assemblies are inherently cytotoxic (7). We analyzed the toxicity of PI3-SH3 fibrils on cultured neuroblastoma cells from the SH-SY5Y cell line. In excellent agreement with bis-ANS binding data, the fibrils formed by PI3-SH3-SS were less toxic than those formed by the PI3-SH3-WT and PI3-SH3-(SH)₂ domains (Fig. 9I).

Extracellular SH3 domains display disulfide bonds and a high sequential intrinsic aggregation propensity

SH3 domains have been considered traditionally as structural elements of multidomain intracellular signaling proteins and devoid of disulfide bonds. However, it has been shown recently that the extracellular melanoma inhibitory activity protein (MIA) consists of a single domain adopting an SH3-fold covalently linked by two intramolecular disulfide bonds. Moreover, three MIA homologous extracellular
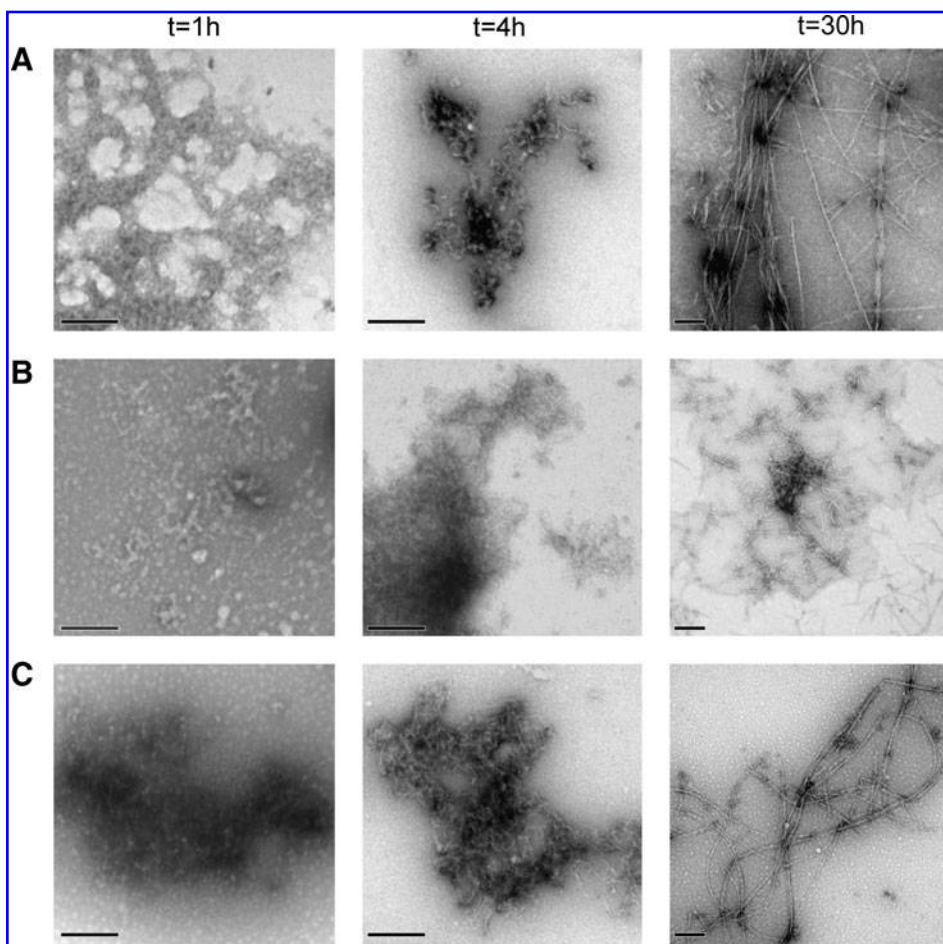
formed by PI3-SH3-WT (61%) and PI3-SH3-(SH)₂ (60%) (Supplementary Table S1). In agreement with these data, PI3-SH3-WT and PI3-SH3-(SH)₂ fibrils exhibit higher binding to bis-ANS than the fibrils formed by the disulfide-containing domain, indicating the existence of a lower proportion of hydrophobic residues exposed to solvent in

FIG. 8. **Transmission electron micrographs of (A) PI3-SH3-WT, (B) PI3-SH3-SS, and (C) PI3-SH3-(SH)₂ negatively stained samples collected at different times along aggregation experiments.** The scale bar represents 200 nm.
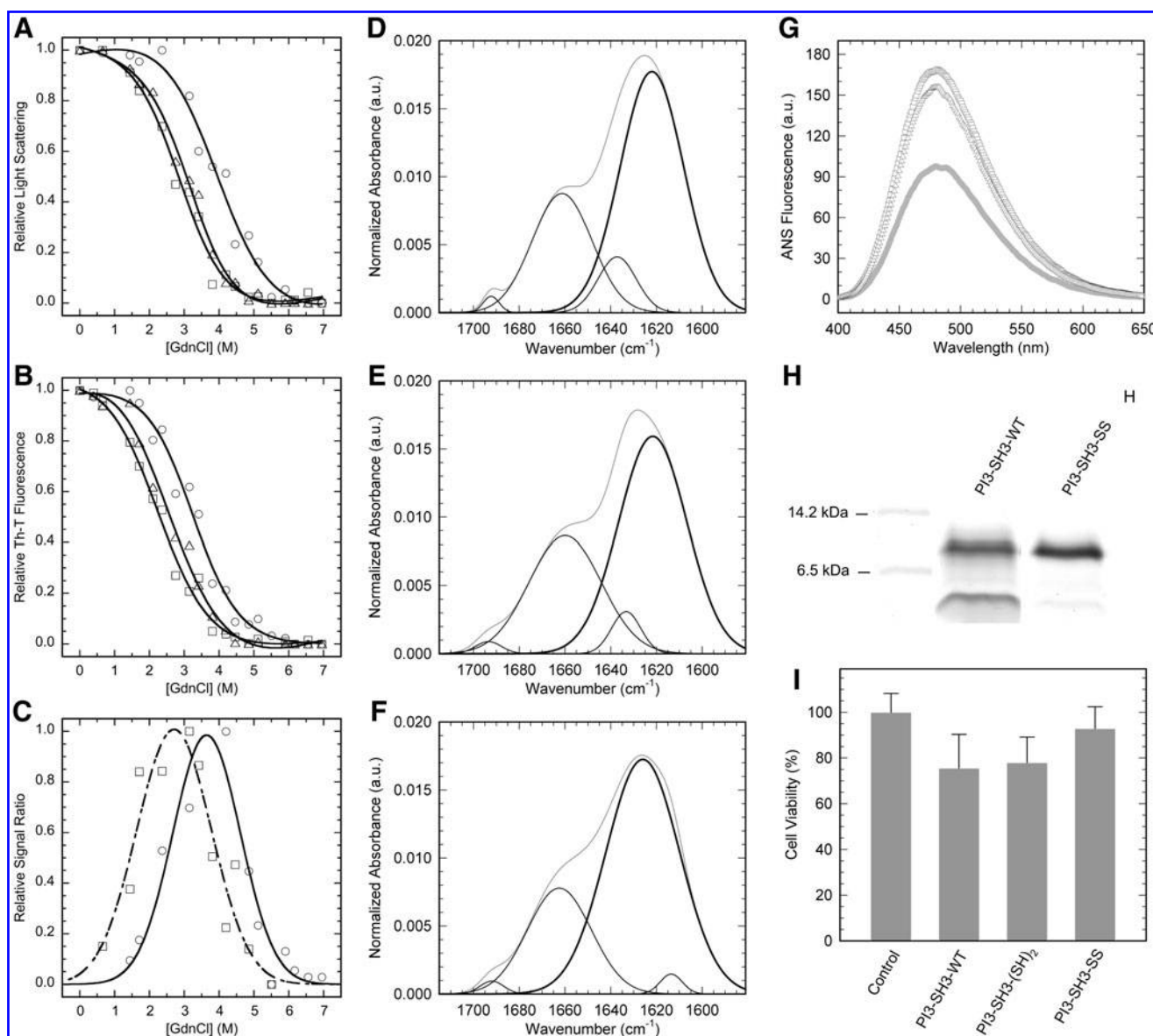
FIG. 9. Conformational and toxic properties of PI3-SH3 domains. (A) Fibrils stability in the presence of Gdn·HCl followed by light scattering. **(B)** Fibrils stability followed by thioflavin-T binding. **(C)** Population of intermediate states. **(D–F)** Attenuated total reflectance–Fourier transformed infrared spectroscopy spectra in the amide I region of PI3-SH3-WT, PI3-SH3-$(SH)_2$, and PI3-SH3-SS (respectively); the thick line indicates the contribution of intermolecular β-sheet to the spectra. **(G)** ANS binding to PI3-SH3 fibrils. **(H)** SDS-PAGE analysis of the proteolytic susceptibility of amyloid fibrils. **(I)** Viability analysis of SH-SY5Y cells exposed to PI3-SH3 amyloid fibrils for 48 h. Error bars indicate $\pm$SE ($n=4$). One hundred percent cell viability was assigned to control samples corresponding to cells incubated in domain free DMEM. In **(A, B, C,** and **G)** *panels* symbols correspond to PI3-SH3-WT (*squares*), PI3-SH3-SS (*circles*), and PI3-SH3-$(SH)_2$ (*triangles*).

proteins with the four conserved Cys have been identified (TANGO, MIA-2, and OTOR) (44). Since our data suggest that the presence of disulfide bonds might modulate the aggregation propensity of SH3 domains, we compared the intrinsic aggregation properties of these extracellular SH3 disulfide-containing domains with those of classical intracellular ones using AGGRESCAN (Fig. 10). The analysis indicates that extracellular SH3 domains display a higher number of aggregation-prone regions in their sequence and support a higher intrinsic aggregation load than intracellular domains.

Discussion

Cyclization increases PI3-SH3 domain stability

Biophysical data indicate that the three PI3-SH3 domains analyzed in the present study exhibit a properly folded conformation in their native states. The dithiol form is slightly more stable than the wild-type domain. DSC data indicate that ΔH is lower, in absolute value, in PI3-SH3-$(SH)_2$ than in PI3-SH3-WT and therefore that stabilization does not arise from the establishment of favorable interactions by the thiol groups but rather from a decrease in ΔS in the mutant form.
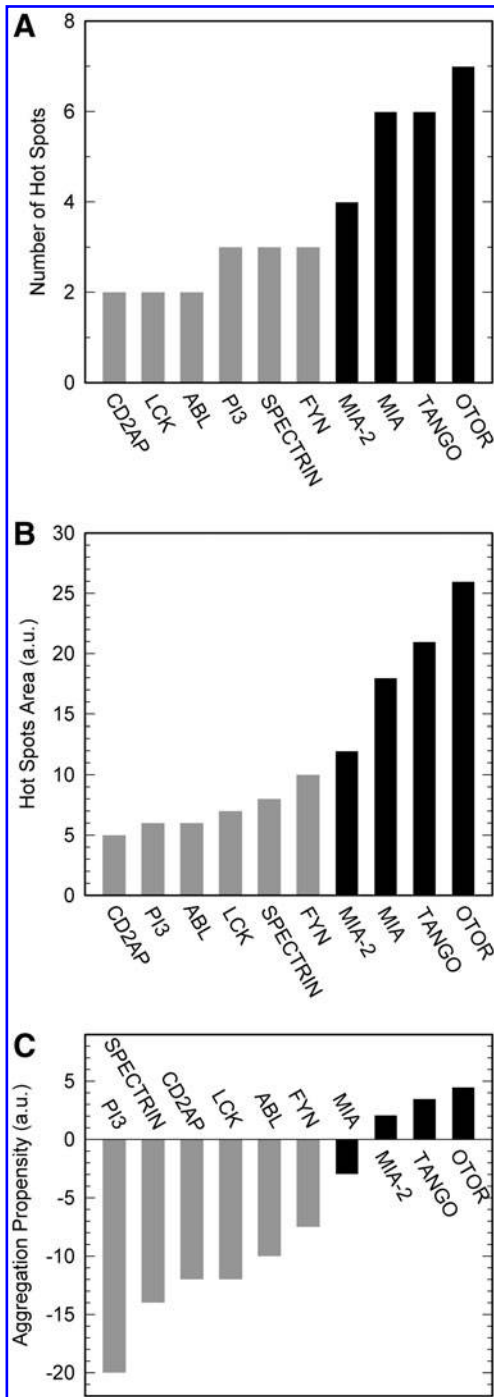
FIG. 10. **Intrinsic aggregation propensities of intracellular (gray) and extracellular (black) SH3 domains.** All extracellular domains share two conserved disulfide bonds. **(A)** Number of aggregation-prone regions in the sequences. **(B)** Area of aggregation-prone regions in the AGGRESCAN profile, reflecting the theoretical aggregation potency of these regions. **(C)** Predicted aggregation propensities of SH3 domains. Higher values indicate higher aggregation propensity.

The ProtSA server (21) indicates that, in the wild-type domain, Ala3 and Ile82 are more exposed to solvent than expected for these hydrophobic residues. Their mutation to Cys displaying polar free thiols in the reduced state would be entropically favorable and might well account for the

observed increase in stability. Oxidative folding experiments confirm that the Cys are exposed to solvent and in a flexible environment in PI3-SH3-(SH)2.

Direct comparison of PI3-SH3-SS with its dithiol form allows differentiating the effect of the mutations from the effect of the disulfide bond. Crosslinking of PI3-SH3 stabilizes the domain against both thermal and chemical denaturation, with an increase in $T_{\rm m}$ of ~ 15 K and a $\Delta\Delta G_{\rm U\text{-}F}$ at 298 K of ~ 3.5 kcal/mol, relative to the dithiol form. It is generally assumed that the stability provided by a disulfide bond results largely from a reduction in the configurational entropy ($\Delta S_{\rm conf}$) of the unfolded state. The $\Delta S_{\rm conf}$ is related to the size of the polypeptide loop enclosed by the disulfide bond (N) and can be approximated theoretically according to the equation (37):

$$\Delta S_{\rm conf} = 2.1\ (3/2)\ {\rm R\ ln\ N} \tag{1}$$

where R is the gas constant.

According to Equation (1) the expected stabilization of PI3-SH3-SS, relative to its reduced form, is 4.5 kcal/mol. Therefore, although the experimentally measured increase in stability is among the highest reported for an SH3 domain (27) it is lower than the theoretical estimate, indicating that loop entropy is not the only factor determining the stability of the cycled domain. Together with a decrease in ΔS, as measured by DSC, the disulfide bond causes a decrease in ΔH, indicating enthalpy–entropy compensation. The same effect has been observed for a number of disulfide mutants, including those of a camelid antibody (29), cytochrome c (4), and barnase (31), demonstrating that the precise thermodynamic effects of introducing a covalent link in a polypeptide are hardly predictable from simple theoretical considerations (16). In these protein models, disulfide bonds tend to decrease the heat capacity change of unfolding ($\Delta C_{\rm p}$). The $\Delta C_{\rm p}$ between the folded and unfolded states of proteins is thought to arise from the exposure of buried side-chains to solvent, with minor contributions from changes in configurational entropy. As proposed by Doig and Williams (20), the 45% decrease in the $\Delta C_{\rm p}$ of PI3-SH3-SS likely results from a more compact unfolded state with restricted hydration of side chains.

Cyclization accelerates PI3-SH3-folding

Cyclization is always expected to increase folding rates due to the larger decrease in configurational entropy of the unfolded state relative to that in the transition state. Unfolding rates will decrease only if the polypeptide termini become apart at the transition state. Connection of the N- and C- termini in PI3-SH3-SS causes a large increase, by over 1 order of magnitude, of the folding rate and has, by contrast, only a small influence on the unfolding rate. This behavior has also been observed for disulfide mutants of barnase (15), subtilisin (45), and acylphosphatase (38). However, cyclization in the structurally homologous SH3 domain of src kinase (src-SH3) domain affected roughly equally its folding and unfolding rates (27), suggesting that its ends are not as structured in the transition state as they are in the native conformation and, likely, that a rate-limiting step in unfolding is the dissociation of the N- and C- termini (27). This view is consistent with the results obtained by Φ analysis for this protein (39) and the spectrin-SH3 domain (34). The two studies indicate that the folding

transition state of these domains involves the association of the distal β-hairpin and the diverging turn, whereas the N and C termini are completely disordered. The low Φ values obtained here for mutants in the β-strands 1 and 5 indicate that the protein ends are also unstructured in the transition state of PI3-SH3-WT, confirming thus a robust energy landscape for the folding of SH3 domains. Cyclization makes the topology of the protein symmetric and tends to reduce the polarization of the transition state. The dissimilar Φ values obtained by circularization and point mutation of N- and C- regions in PI3-SH3 indicate that the free energy landscape of this particular domain is severely affected by the disulfide bond promoted topology change, confirming that despite the folding landscape of this protein family is relatively insensitive to sequential variations it is sensitive to topological constrains (26).

Cyclization slows down PI3-SH3 aggregation

The effect of polypeptide chain crosslinking in amyloid fibril formation is still poorly understood. Disulfide crosslinking does not prevent self-association into amyloid structures. Therefore, the conformational restrictions introduced by the covalent bond do not prevent the accommodation of the polypeptide backbone into the highly ordered cross-β-sheet structure characteristic of amyloid fibrils. However, it strongly decreases the nucleation and elongation rates, slowing down the lag phase as well as the overall aggregation reaction. The aggregation of PI3-SH3-WT has been shown to be consistent with the nucleated conformational conversion mechanism (8), in which initially soluble monomers coalesce to form amorphous assemblies that later reorganize into ordered oligomers and finally β-sheet enriched amyloid fibrils (43). Hydrophobic forces are thought to drive the initial unspecific condensation of monomers into amorphous oligomers. According to the conformational properties and hydrophobic residues clustering of PI3-SH3-SS and PI3-SH3-$(SH)_2$ domains, there is not obvious reason to assume differences in their association rates at this stage. Upon the initial collapse, polypeptides within the disordered oligomers realign slowly to establish hydrogen bonds that favor the formation of β-sheets. The dynamic flexibility of the polypeptide chain might play an important role in this second step, since multiple rounds of association and dissociation between adjacent protein regions likely occur during the lag phase, before an initially ordered and stable enough β-sheet conformation is attained (2). The reduced flexibility of PI3-SH3-SS might difficult this rearrangement stage delaying the formation of productive oligomers, resulting in a lower k_n.

The elongation step in amyloid formation is thought to involve a "dock and lock" mechanism, in which a significant conformational rearrangement of incoming monomers is necessary before they become incorporated into preformed fibrils (17). The slower elongation rate of PI3-SH3-SS suggests that dynamic protein flexibility might be also important at the polymerization stage.

Cyclization reduces the toxicity of PI3-SH3 amyloid assemblies

High-resolution MAS NMR analysis has allowed Bayro *et al*. to propose a structural model for PI3-SH3-WT amyloid fibrils (3). In the model, four β-sheets form the core of two distinct protofilaments and lateral contacts between PI3-SH3-WT subunits in adjacent protofilaments allow their association to form the fibrils (Supplementary Fig. S2). The N-terminus adopts a rigid β-strand structure in the core of the fibril. In contrast, the C-terminal residues appear to be dynamically and structurally disordered and located in the two external sides of the fibril (3). Restriction of the C-end entropy by crosslinking might allow its integration in the core β-sheet structure (Supplementary Fig. S2). This would explain the highest stability of the β-sheet structure in PI3-SH3-SS fibrils, the insensitivity of these fibrils to highly reducing conditions, the higher proportion of intermolecular β-sheet and the resistance of fibrils to proteolysis, as well as the reduced exposition of hydrophobic residues to solvent. This cyclization-promoted structural gain has a crucial functional consequence: it significantly reduces the cytotoxicity of the resulting fibrils.

Materials and Methods

Disulfide bond design

A PI3-SH3 domain with the N and C terminal regions linked by a disulfide bridge (PI3-SH3-SS) was designed using FoldX (version 2.65) (http://foldx.crg.es/) (42). The best positions to introduce the Cys residues were identified employing the BuildModel command, which calculates the relative stability difference by rotating the same residues in the wild-type and mutant structures according to the FoldX rotamer database. The atomic spatial coordinates of PI3-SH3-WT in the crystal structure (1PHT.pdb) were used as input.

Cloning, mutagenesis, and expression

The PI3-SH3-WT protein consists of 83 residues from the SH3 domain of bovine PI3-kinase plus a Met at the N-terminus. Its cDNA was cloned in pBAT-4 (46). The Ala3 and Ile82 residues were mutated to Cys, the resulting plasmid was transformed in BL21(DE3) *Escherichia coli* cells and the proteins were expressed and purified as described previously (46). The mutant cDNA was sequenced and the protein identity was checked by mass spectrometry. Gel filtration chromatography indicated that the mutant protein is a monomer. Unless otherwise indicated, experiments were performed in 50 mM sodium phosphate at pH 7.0 (buffer-N).

Disulfide crosslinking and reduction

To confirm the formation of the designed disulfide bond, PI3-SH3-SS was incubated in 0.1 M Tris-HCl buffer, pH 8.5, containing 0.1 M 4-vinylpyridine for 1 h at room temperature, diluted 1:10 in 0.1% aqueous trifluoroacetic acid, and analyzed by MALDI-TOF MS in an Ultraflex spectrometer (Bruker). When required, the disulfide bond was reduced by incubation in the presence of 10 mM DTT or Tris (2-carboxyethyl)phosphine (TCEP) for at least 1 h.

Oxidative folding and reductive unfolding

For oxidative folding experiments PI3-SH3-SS was reduced and unfolded in 0.5 M Tris buffer pH 8.4, containing 10 mM DTT and 7 M guanidinium chloride for 2 h at room temperature. To initiate folding, the sample was loaded onto a

desalting column equilibrated with 0.1 M Tris buffer, pH 8.4. The protein was eluted in the same buffer to a final protein concentration of 0.3 mg/ml, in the absence and in the presence of 0.5 mM GSSG. Folding species were trapped in a time-course manner by alkylation with 0.1 M sodium iodoacetate for 2 min at room temperature. The trapped intermediates were subsequently analyzed by SDS-PAGE under non-denaturing conditions. For reductive unfolding experiments PI3-SH3-SS (0.5 mg/ml) was dissolved at room temperature in 0.1 M Tris buffer, pH 8.4, containing 1 mM DTT and the species were trapped and analyzed as described above.

Circular dichroism

CD spectra were measured in a Jasco-710 spectro-polarimeter thermostated at 298 K. Spectra were recorded from 260 to 205 nm, at 1 nm intervals, 1 nm bandwidth, and a scan speed of 10 nm/min. Twenty accumulations were averaged for each spectrum. Protein concentrations were 20 μM in buffer-N. Thermal denaturation was monitored at 235 nm each 0.1 K, with 2 min temperature equilibrium between measures. Experimental data were fitted to a two-state transition curve for which the signals of the folded and unfolded states are dependent on the temperature using the nonlinear least squares algorithm provided with Kaleidagraph (Abel-beck Software).

Intrinsic fluorescence

Fluorescence was measured in a Varian Cary Eclipse spectrofluorometer using an excitation wavelength of 268 nm. Slit widths were typically 5 nm for excitation and 10 nm for emission. Spectra were acquired at 1 nm intervals, a 600 nm/min rate, and 0.1 s averaging time.

In PI3-SH3 domains, Trp55 is exposed to solvent and its fluorescence exhibits a linear dependence on the temperature or chaotropic agents concentration. Tyr residues are responsive to conformational changes, but their signal is strongly influenced by the fluorescence of Trp55. The ratio 303/350 nm provides an accurate measurement of structural changes in PI3-SH3 domains. Thermal denaturation was analyzed in buffer-N at 20 μM protein concentration each 0.1 K with 2 min equilibration between measures. For chemical denaturation the native protein was dissolved at 20 μM in buffer-N containing selected concentrations of denaturants (0–9 M urea or Gdn·HCl). The reaction was equilibrated for 20 h at room temperature. Experimental data were fitted as described for CD measurements.

Differential scanning calorimetry

The heat capacity of PI3-SH3 as a function of temperature was measured with a high-sensitivity differential scanning VP-DSC microcalorimeter (MicroCal). Protein samples and reference solutions were properly degassed and carefully loaded into the cells to avoid bubble formation. Thermal denaturation scans were performed with freshly prepared buffer-exchanged protein solutions. The baseline of the instrument was routinely recorded before the experiments. Experiments were performed in buffer-N, at a scanning rate of 1 K/min. Experiments were carried out with 40–50 μM of protein. Thermal denaturations were reversible (as judged by the agreement of the thermogram shapes and sizes between the first and the second scans). Pre- and post-transition baselines were considered linear with temperature.

A model-free analysis indicated that the calorimetric enthalpy is equal to the van't Hoff enthalpy, within experimental error. Therefore, protein stability parameters were obtained by analyzing thermal scans considering a two-state unfolding model using software developed in our laboratory implemented in Origin 7 (OriginLab). The unfolding thermo-dynamic parameters are not influenced by the ionization properties of the buffer as long as the pH of the experiment is close to the buffer pKa (7.2 for phosphate), and the buffer ionization enthalpy is small (0.86 kcal/mol for phosphate).

NMR spectroscopy

Samples were prepared at 40 μM in buffer-N, using a 9:1 H_2O/D_2O. One-dimensional NMR spectra were acquired at selected temperatures on a Bruker AVANCE 600-MHz spectrometer using solvent suppression WATERGATE techniques. The collected spectra were processed and analyzed using the TopSpinv2.0 software packages from Bruker Biospin. The area under the NMR signals at the aliphatic region (form 10 to 5 ppm) was calculated and plotted to follow the temperature-induced denaturation of PI3-SH3 domains.

Determination of folding kinetic parameters

The kinetics of the folding and unfolding reactions at 298 K were followed in a Bio-Logic SFM-3 stopped-flow instrument using excitation at 268 and a 300 nm fluorescence cut-off filter. Starting with the protein in buffer-N, the unfolding reaction was promoted by dilution with appropriate volumes of the same buffer containing 9.5 M urea. For the folding reaction, appropriate volumes of urea-free buffer were added to an initial protein solution in buffer-N containing 9.5 M urea. Kinetic traces were fitted to single-exponential functions and the resulting rate constants to a two-state transition equation to determine the kinetic and free energy values:

$$\Delta G_{F\text{-}U} = RT \ln (k_f/k_u)$$

where k_f and k_u are the rates of folding and unfolding, respectively, at denaturant concentrations experimentally accessible for the domain. The differences in the free energy of unfolding ($\Delta\Delta G_{F\text{-}U}$) between the wild-type protein and each mutant are calculated as:

$$\Delta\Delta G_{F\text{-}U}(\Delta G_{F\text{-}U})_{wt} - (\Delta G_{F\text{-}U})_{mut} = \Delta\Delta G_{\ddagger\text{-}U} - \Delta\Delta G_{\ddagger\text{-}F}$$
$$\Delta\Delta G_{\ddagger\text{-}U} = RT \ln (k_f^{wt}/k_f^{mut})$$
$$\Delta\Delta G_{\ddagger\text{-}F} = RT \ln (k_u^{wt}/k_u^{mut})$$

The parameter Φ_F is defined as:

$$\Phi_F = \Delta\Delta G_{\ddagger\text{-}U}/\Delta\Delta G_{F\text{-}U}$$

and is interpreted as the fraction of the mutated residue's interactions that are formed in the transition state.

Amyloid fibril formation

Lyophilized PI3-SH3 domains were dissolved in buffer-N at 7 mg/ml. After filtration through a 0.22 μm filter to remove

residual aggregates, protein solutions were diluted to 3.5 mg/ml adding an equal volume of 50 mM glycine, and the pH adjusted immediately with 5 M HCl to pH 2.0. Fibril formation was promoted by incubating the samples at 298 K and 500 rpm agitation. The 10 mM TCEP was used as reducing agent in these experiments.

Aggregation kinetics

After different incubation intervals samples were diluted in glycine buffer containing 60 μM Thioflavin-T (Th-T) and equilibrated 5 min at 298 K. They were excited at 450 nm and the fluorescence emission spectrum recorded between 470 and 600 nm with slit widths of 5 and 10 nm for excitation and emission, respectively. The kinetic parameters for the aggregation process were calculated according to an autocatalytic reaction, as previously described (40).

bis-ANS binding

The fluorescence emission of bis-ANS was recorded at 298 K. Protein samples (40 μM) at pH 7.0 or pH 2.0 were diluted tenfold into the corresponding buffer containing bis-ANS (2.6 μM). Spectra were collected after 5 min incubation. The samples were excited at 365 nm and emission measured between 440 and 640 nm with slit widths of 5 and 10 nm for excitation and emission, respectively.

Electron microscopy

Aggregated protein samples were diluted 20 times in the same buffer, 10 μl placed on a carbon-coated copper grid and allowed to stand for 5 min. The grid was washed with distilled water and the sample stained with 2% uranyl acetate for 1 min. The samples were imaged in a Hitachi H-7000 transmission electron microscope operating at an accelerating voltage of 75 kV.

Amyloid fibrils chemical denaturation

Mature fibril solutions were incubated in 0–7 M Gdn·HCl at pH 2 and for 16 h. Subsequently, they were diluted in glycine buffer containing 60 μM Th-T. The changes in light scattering at 340 nm and Th-T fluorescence at 480 nm were followed with a Varian Cary Eclipse spectrofluorimeter. Experimental data were fitted as described for CD measurements.

Limited proteolysis

Limited proteolysis was performed using pepsin in 50 mM glycine buffer at pH 2.0 and 298 K using an E/S ratio of 1:200 (by weight). The reactions were quenched after 5 min by adding an appropriate volume of 5 M NaOH. The proteolytic mixtures were analyzed by SDS-PAGE.

Attenuated total reflectance–Fourier transformed infrared spectroscopy

ATR-FTIR analyses of SH3 aggregates were performed using a Bruker Tensor 27 FTIR Spectrometer (Bruker Optics) with a Golden Gate MKII ATR accessory as previously described (41).

Cell viability assays

The toxicity of PI3-SH3 aggregates (10 μM) was analyzed on cultured neuroblastoma cells (SH-SY5Y cell line) by measuring formazan formation by mitochondrial dehydrogenases as previously described (41). Four independent assays were performed for each protein sample.

Author Disclosure Statement

No competing financial interests exist.

References

1. Arolas JL, D'Silva L, Popowicz GM, Aviles FX, Holak TA, and Ventura S. NMR structural characterization and computational predictions of the major intermediate in oxidative folding of leech carboxypeptidase inhibitor. *Structure* 13: 1193–1202, 2005.
2. Auer S, Meersman F, Dobson CM, and Vendruscolo M. A generic mechanism of emergence of amyloid protofilaments from disordered oligomeric aggregates. *PLoS Comput Biol* 4: e1000222, 2008.
3. Bayro MJ, Maly T, Birkett NR, Macphee CE, Dobson CM, and Griffin RG. High-resolution MAS NMR analysis of PI3-SH3 amyloid fibrils: backbone conformation and implications for protofilament assembly and structure. *Biochemistry* 49: 7474–7484, 2010.
4. Betz SF and Pielak GJ. Introduction of a disulfide bond into cytochrome c stabilizes a compact denatured state. *Biochemistry* 31: 12337–12344, 1992.
5. Bolognesi B, Kumita JR, Barros TP, Esbjorner EK, Luheshi LM, Crowther DC, Wilson MR, Dobson CM, Favrin G, and Yerbury JJ. ANS binding reveals common features of cytotoxic amyloid species. *ACS Chem Biol* 5: 735–740, 2010.
6. Booth DR, Sunde M, Bellotti V, Robinson CV, Hutchinson WL, Fraser PE, Hawkins PN, Dobson CM, Radford SE, Blake CC, and Pepys MB. Instability, unfolding and aggregation of human lysozyme variants underlying amyloid fibrillogenesis. *Nature* 385: 787–793, 1997.
7. Bucciantini M, Giannoni E, Chiti F, Baroni F, Formigli L, Zurdo J, Taddei N, Ramponi G, Dobson CM, and Stefani M. Inherent toxicity of aggregates implies a common mechanism for protein misfolding diseases. *Nature* 416: 507–511, 2002.
8. Carulla N, Zhou M, Arimon M, Gairi M, Giralt E, Robinson CV, and Dobson CM. Experimental characterization of disordered and ordered aggregates populated during the process of amyloid fibril formation. *Proc Natl Acad Sci U S A* 106: 7828–7833, 2009.
9. Cascales L and Craik DJ. Naturally occurring circular proteins: distribution, biosynthesis and evolution. *Org Biomol Chem* 8: 5035–5047, 2010.
10. Castillo V, Espargaro A, Gordo V, Vendrell J, and Ventura S. Deciphering the role of the thermodynamic and kinetic stabilities of SH3 domains on their aggregation inside bacteria. *Proteomics* 10: 4172–4185, 2010.
11. Castillo V, Grana-Montes R, Sabate R, and Ventura S. Prediction of the aggregation propensity of proteins from the primary sequence: aggregation properties of proteomes. *Biotechnol J* 6: 674–685, 2011.

12. Castillo V and Ventura S. Amyloidogenic regions and interaction surfaces overlap in globular proteins related to conformational diseases. *PLoS Comput Biol* 5: e1000476, 2009.

13. Chiti F and Dobson CM. Protein misfolding, functional amyloid, and human disease. *Annu Rev Biochem* 75: 333–366, 2006.

14. Chiti F and Dobson CM. Amyloid formation by globular proteins under native conditions. *Nat Chem Biol* 5: 15–22, 2009.

15. Clarke J and Fersht AR. Engineered disulfide bonds as probes of the folding pathway of barnase: increasing the stability of proteins against the rate of denaturation. *Biochemistry* 32: 4322–4329, 1993.

16. Clarke J, Hounslow AM, and Fersht AR. Disulfide mutants of barnase. II. Changes in structure and local stability identified by hydrogen exchange. *J Mol Biol* 253: 505–513, 1995.

17. Collins SR, Douglass A, Vale RD, and Weissman JS. Mechanism of prion propagation: amyloid growth occurs by monomer addition. *PLoS Biol* 2: e321, 2004.

18. Conchillo-Sole O, de Groot NS, Aviles FX, Vendrell J, Daura X, and Ventura S. AGGRESCAN: a server for the prediction and evaluation of "hot spots" of aggregation in polypeptides. *BMC Bioinformatics* 8: 65, 2007.

19. Creighton TE and Goldenberg DP. Kinetic role of a metastable native-like two-disulphide species in the folding transition of bovine pancreatic trypsin inhibitor. *J Mol Biol* 179: 497–526, 1984.

20. Doig AJ and Williams DH. Is the hydrophobic effect stabilizing or destabilizing in proteins? The contribution of disulphide bonds to protein stability. *J Mol Biol* 217: 389–398, 1991.

21. Estrada J, Bernado P, Blackledge M, and Sancho J. ProtSA: a web application for calculating sequence specific protein solvent accessibilities in the unfolded ensemble. *BMC Bioinformatics* 10: 104, 2009.

22. Fandrich M, Fletcher MA, and Dobson CM. Amyloid fibrils from muscle myoglobin. *Nature* 410: 165–166, 2001.

23. Fernandez-Busquets X, de Groot NS, Fernandez D, and Ventura S. Recent structural and computational insights into conformational diseases. *Curr Med Chem* 15: 1336–1349, 2008.

24. Foss TR, Wiseman RL, and Kelly JW. The pathway by which the tetrameric protein transthyretin dissociates. *Biochemistry* 44: 15525–15533, 2005.

25. Goldenberg DP and Creighton TE. Folding pathway of a circular form of bovine pancreatic trypsin inhibitor. *J Mol Biol* 179: 527–545, 1984.

26. Grantcharova VP and Baker D. Circularization changes the folding transition state of the src SH3 domain. *J Mol Biol* 306: 555–563, 2001.

27. Grantcharova VP, Riddle DS, and Baker D. Long-range order in the src SH3-folding transition state. *Proc Natl Acad Sci U S A* 97: 7084–7089, 2000.

28. Guijarro JI, Sunde M, Jones JA, Campbell ID, and Dobson CM. Amyloid fibril formation by an SH3 domain. *Proc Natl Acad Sci U S A* 95: 4224–4228, 1998.

29. Hagihara Y, Mine S, and Uegaki K. Stabilization of an immunoglobulin fold domain by an engineered disulfide bond at the buried hydrophobic region. *J Biol Chem* 282: 36489–36495, 2007.

30. Jahn TR and Radford SE. Folding versus aggregation: polypeptide conformations on competing pathways. *Arch Biochem Biophys* 469: 100–117, 2008.

31. Johnson CM, Oliveberg M, Clarke J, and Fersht AR. Thermodynamics of denaturation of mutants of barnase with disulfide crosslinks. *J Mol Biol* 268: 198–208, 1997.

32. Krittanai C and Johnson WC. Correcting the circular dichroism spectra of peptides for contributions of absorbing side chains. *Anal Biochem* 253: 57–64, 1997.

33. Liang J, Chen JK, Schreiber ST, and Clardy J. Crystal structure of P13K SH3 domain at 20 angstroms resolution. *J Mol Biol* 257: 632–643, 1996.

34. Martinez JC and Serrano L. The folding transition state between SH3 domains is conformationally restricted and evolutionarily conserved. *Nat Struct Biol* 6: 1010–1016, 1999.

35. Maurer-Stroh S, Debulpaep M, Kuemmerer N, Lopez de la Paz M, Martins IC, Reumers J, Morris KL, Copland A, Serpell L, Serrano L, Schymkowitz JW, and Rousseau F. Exploring the sequence determinants of amyloid structure using position-specific scoring matrices. *Nat Methods* 7: 237–242, 2010.

36. Mossuto MF, Bolognesi B, Guixer B, Dhulesia A, Agostini F, Kumita JR, Tartaglia GG, Dumoulin M, Dobson CM, and Salvatella X. Disulfide bonds reduce the toxicity of the amyloid fibrils formed by an extracellular protein. *Angew Chem Int Ed Engl* 50: 7048–7051, 2011.

37. Pace CN, Grimsley GR, Thomson JA, and Barnett BJ. Conformational stability and activity of ribonuclease T1 with zero, one, and two intact disulfide bonds. *J Biol Chem* 263: 11820–11825, 1988.

38. Parrini C, Bemporad F, Baroncelli A, Gianni S, Travaglini-Allocatelli C, Kohn JE, Ramazzotti M, Chiti F, and Taddei N. The folding process of acylphosphatase from *Escherichia coli* is remarkably accelerated by the presence of a disulfide bond. *J Mol Biol* 379: 1107–1118, 2008.

39. Riddle DS, Grantcharova VP, Santiago JV, Alm E, Ruczinski I, and Baker D. Experiment and theory highlight role of native state topology in SH3-folding. *Nat Struct Biol* 6: 1016–1024, 1999.

40. Sabate R, Castillo V, Espargaro A, Saupe SJ, and Ventura S. Energy barriers for HET-s prion forming domain amyloid formation. *FEBS J* 276: 5053–5064, 2009.

41. Sabate R, Espargaro A, de Groot NS, Valle-Delgado JJ, Fernandez-Busquets X, and Ventura S. The role of protein sequence and amino acid composition in amyloid formation: scrambling and backward reading of IAPP amyloid fibrils. *J Mol Biol* 404: 337–352, 2010.

42. Schymkowitz J, Borg J, Stricher F, Nys R, Rousseau F, and Serrano L. The FoldX web server: an online force field. *Nucleic Acids Res* 33: W382–W388, 2005.

43. Serio TR, Cashikar AG, Kowal AS, Sawicki GJ, Moslehi JJ, Serpell L, Arnsdorf MF, and Lindquist SL. Nucleated conformational conversion and the replication of conformational information by a prion determinant. *Science* 289: 1317–1321, 2000.

44. Stoll R and Bosserhoff A. Extracellular SH3 domain containing proteins—features of a new protein family. *Curr Protein Peptide Sci* 9: 221–226, 2008.

45. Strausberg S, Alexander P, Wang L, Gallagher T, Gilliland G, and Bryan P. An engineered disulfide cross-link accelerates the refolding rate of calcium-free subtilisin by 850-fold. *Biochemistry* 32: 10371–10377, 1993.

46. Ventura S, Lacroix E, and Serrano L. Insights into the origin of the tendency of the PI3-SH3 domain to form amyloid fibrils. *J Mol Biol* 322: 1147–1158, 2002.

47. Wani AH and Udgaonkar JB. Revealing a concealed intermediate that forms after the rate-limiting step of refolding of the SH3 domain of PI3 kinase. *J Mol Biol* 387: 348–362, 2009.

48. Zavodszky M, Chen CW, Huang JK, Zolkiewski M, Wen L, and Krishnamoorthi R. Disulfide bond effects on protein

stability: designed variants of Cucurbita maxima trypsin inhibitor-V. *Protein Sci* 10: 149–160, 2001.

49. Zhou HX. Effect of backbone cyclization on protein folding stability: chain entropies of both the unfolded and the folded states are restricted. *J Mol Biol* 332: 257–264, 2003.

Address correspondence to:
Prof. Salvador Ventura
Departament de Bioquímica i Biologia Molecular
Institut de Biotecnologia i de Biomedicina
Universitat Autònoma de Barcelona
Bellaterra 08193 (Barcelona)
Spain

E-mail: salvador.ventura@uab.es

Abbreviations Used

ΔC_p = heat capacity change of unfolding
ATR-FTIR = attenuated total reflectance–Fourier transformed infrared spectroscopy
bis-ANS = 4,4′-dianilino-1,1′-binaphthyl-5,5′-disulfonic acid
CD = circular dichroism
DSC = differential scanning calorimetry
DTT = dithiothreitol
Gdn·HCl = guanidine hydrochloride
MALDI-TOF MS = matrix-assisted laser desorption/ionization-time of flight mass spectrometry
MIA = melanoma inhibitory activity protein
PI3-SH3 = SH3 domain of p85α subunit of bovine phosphatidyl-inositol-3′-kinase
SH3 = SRC homology 3 domain
src-SH3 = SH3 domain of src kinase
TCEP = Tris (2-carboxyethyl)phosphine
Th-T = thioflavin-T

This article has been cited by:

1. Jianwei He, Linan Xu, Zhiyuan Zou, Nobuhiro Ueyama, Hui Li, Akio Kato, Gary W. Jones, Youtao Song. 2012. Molecular dynamics simulation to investigate the impact of disulfide bond formation on conformational stability of chicken cystatin I66Q mutant. *Journal of Biomolecular Structure and Dynamics* 1-10. [CrossRef]
2. Raimon Sabate, Alba Espargaro, Ricardo Graña-Montes, David Reverter, Salvador Ventura. 2012. Native Structure Protects SUMO Proteins from Aggregation into Amyloid Fibrils. *Biomacromolecules* 120525092553002. [CrossRef]